

Research paper

A new approach to discern the hydrocarbon sources (oil vs. methane) of authigenic carbonates forming at marine seeps



Yuedong Sun^{a,d,f,g}, Shanggui Gong^{c,*}, Niu Li^{a,f}, Jörn Peckmann^d, Meng Jin^{a,f,g}, Harry H. Roberts^e, Duofu Chen^{b,c}, Dong Feng^{b,c,**}

^a CAS Key Laboratory of Ocean and Marginal Sea Geology, South China Sea Institute of Oceanology, Chinese Academy of Sciences, Guangzhou, 510301, China

^b Laboratory for Marine Mineral Resources, Qingdao National Laboratory for Marine Science and Technology, Qingdao, 266061, China

^c Shanghai Engineering Research Center of Hadal Science and Technology, College of Marine Sciences, Shanghai Ocean University, Shanghai, 201306, China

^d Institute for Geology, Center for Earth System Science and Sustainability, Universität Hamburg, 20146, Hamburg, Germany

^e Coastal Studies Institute, College of the Coastal and Environment, Louisiana State University, Baton Rouge, LA, 70803, USA

^f Innovation Academy of South China Sea Ecology and Environmental Engineering, Chinese Academy of Sciences, Guangzhou, 510301, China

^g University of Chinese Academy of Sciences, Beijing, 100049, China

ARTICLE INFO

Keywords:
Oil seep
Methane seep
Authigenic carbonate
Organic matter
Carbon isotopes
Sulfur isotopes
Organic sulfur

ABSTRACT

Numerous marine hydrocarbon seeps have been discovered in the past three decades, the majority of which are dominated by methane-rich fluids. However, an increasing number of modern oil seeps and a few ancient oil-seep deposits have been recognized in recent years. Oil seepage exerts significant control on the composition of the seep-dwelling fauna and may have impacted the marine carbon cycle through geological time to a greater extent than previously recognized. Yet, distinguishing oil-seep from methane-seep deposits is difficult in cases where $\delta^{13}\text{C}_{\text{carb}}$ values are higher than approximately $-30\text{\textperthousand}$ due to mixing of different carbon sources. Here, we present a comparative study of authigenic carbonates from oil-dominated (site GC232) and methane-dominated (site GC852) seep environments of the northern Gulf of Mexico, aiming to determine the geochemical characteristics of the two types of seep carbonates. We analyzed (1) major and trace element compositions of carbonates, (2) total organic carbon (TOC), total nitrogen (TN) and carbon isotope ($\delta^{13}\text{C}_{\text{TOC}}$) of residue after decalcification, (3) sulfur isotope signatures of chromium reducible sulfur (CRS, $\delta^{34}\text{S}_{\text{CRS}}$) and residue after CRS extraction ($\delta^{34}\text{S}_{\text{TOS}}$), as well as (4) sulfur contents (TOS) of residue after CRS extraction. Carbonates from the studied oil seep are dominated by aragonite and exhibit lower $\delta^{34}\text{S}_{\text{CRS}}$ values, suggesting carbonate precipitation close to the sediment surface. In addition, oil-seep carbonates are characterized by higher TOC and TOS contents and higher TOC/TN ratios, as well as less negative $\delta^{13}\text{C}_{\text{TOC}}$ values compared to methane-seep carbonates, probably reflecting a contribution of residual crude oil enclosed in oil-seep carbonates. Very low $\delta^{13}\text{C}_{\text{TOC}}$ values (as low as $-68.7\text{\textperthousand}$, VPDB) and low TOC/TN ratios of methane-seep carbonates indicate that the enclosed organic matter is derived mainly from the biomass of methanotrophic biota. This study presents new geochemical data that will allow the discrimination of oil-seep from methane-seep deposits. Although some of the geochemical patterns are likely to be affected by late diagenesis, if applied with caution, such patterns can be used to discern the two end-member types of seepage – oil seeps and methane seeps – in the geological record.

1. Introduction

Hydrocarbon-rich fluid seepage occurs along the continental margins worldwide (Ceramicola et al., 2018; Suess, 2018). Modern seeps are dominated by leakage of methane (Suess, 2018). Besides methane seeps, oil seeps have been reported to occur along continental margins and in deeper basins, such as offshore southern California (Valentine

et al., 2010), the Gulf of Mexico (GoM; e.g., MacDonald et al., 2004), the Black Sea (Körber et al., 2014), and the Brazilian Margin (Freire et al., 2017). In addition, numerous Phanerozoic seep deposits have been shown to be characterized by expulsion of higher hydrocarbons and crude oil (Peckmann et al., 1999; 2001, 2007, 2013; Agirrezabala, 2009). At oil seeps, crude oil tends to cover the seafloor and to fill the pore space of sediment. Certain epifaunal chemosymbiotic taxa dwell in

* Corresponding author.

** Corresponding author. Laboratory for Marine Mineral Resources, Qingdao National Laboratory for Marine Science and Technology, Qingdao, 266061, China.

E-mail addresses: sggong@shou.edu.cn (S. Gong), dfeng@shou.edu.cn (D. Feng).

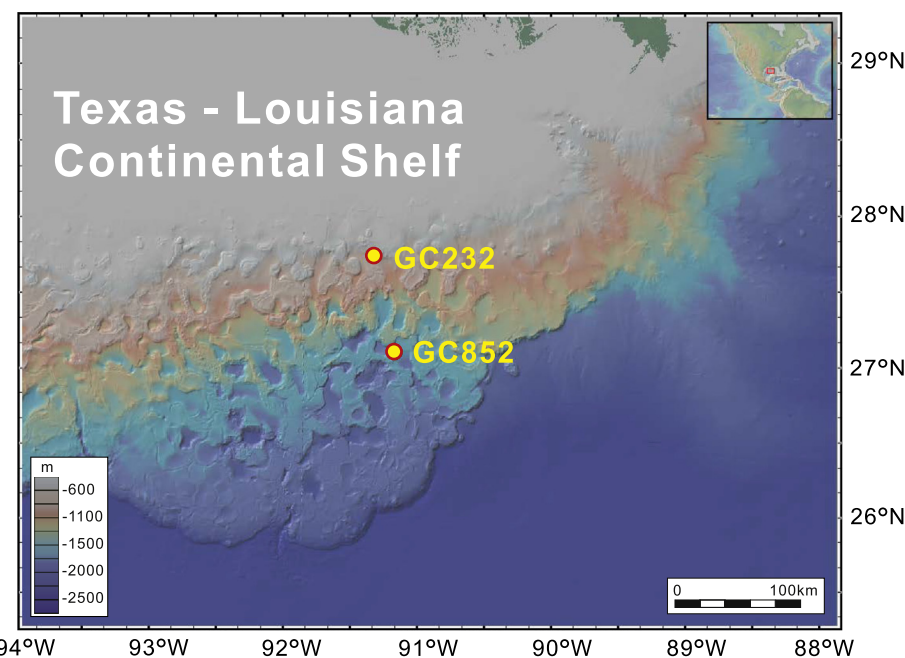


Fig. 1. Location of sites GC232 and GC852 in the northern Gulf of Mexico. Maps were created using GeoMapApp software.

oil seep environments, but infaunal taxa do not tolerate the viscosity of oil and the toxicity of many of its components (cf. Smrzka et al., 2016, 2019). Oil and accessory methane escaping from the seabed facilitate bacterioplankton growth in the bottom water at seeps, which is believed to have provided the nutrition for seep-dwelling dimerelloid brachiopods (Kiel and Peckmann, 2019). The dimerelloid brachiopods of many Paleozoic and Mesozoic seeps with their epifaunal life style would have been better adapted to oil seeps than many of the predominantly infaunal modern and Cenozoic seep taxa (Smrzka et al., 2016). In fact, some of the Paleozoic and Mesozoic seeps typified by mass occurrences of dimerelloid brachiopods may have represented oil rather than methane seeps (Peckmann et al., 2001, 2007, 2011, 2013). Moreover, the occurrence of oil in seep fluids governs chemosynthesis-based symbiosis between seep-endemic metazoans and their symbionts (Rubin-Blum et al., 2017).

Oil seepage exerts a strong selective pressure on bacterial communities in marine sediments (Lamontagne et al., 2004; Orcutt et al., 2010). This selective pressure could, in turn, control the effects of oil on other biota in the vicinity of marine hydrocarbon seeps (Lamontagne et al., 2004). Finally, natural oil seeps not only contribute a significant source of oil to the ocean, they also typically release large quantities of methane to the ocean (Valentine et al., 2010). Oil seepage accompanied by methane will thus increase the methane flux to the ocean and even the atmospheric with the protection of surface coatings on gas bubbles (Valentine et al., 2010). Therefore, the unambiguous identification of oil seeps is imperative to understand the adaption of chemosynthesis-based life to this environment and to better constrain the impact of oil seepage on carbon cycling through geological time.

However, such identification of ancient oil seeps is difficult (e.g., Squires and Gring, 2016). At oil seeps, the increase of alkalinity resulting from microbial anaerobic oxidation of methane (AOM) and the oxidation of higher hydrocarbons (propane, butane; Musat, 2015) as well as other oil components (hexadecane; Mbadinga et al., 2011) leads to carbonate precipitation (cf. Joye et al., 2004; Smrzka et al., 2016). Because methane is strongly depleted in ^{13}C , carbon stable isotope compositions of carbonate ($\delta^{13}\text{C}_{\text{carb}}$) and of lipid biomarkers represent the best tracers of this carbon source (Peckmann and Thiel, 2004; Campbell, 2006). Oil tends to be less ^{13}C depleted than methane, but like methane also oil components can have different $\delta^{13}\text{C}$ values due to

variable sources of the original organic matter and different maturities (Sofer, 1984). Biomarkers may be erased as a function of thermal maturity and variable degrees of mixing of different carbon sources may prevent unambiguous identification of hydrocarbon-seep carbonates by $\delta^{13}\text{C}_{\text{carb}}$ values (Peckmann and Thiel, 2004). Furthermore, characteristic biomarkers of oil-degrading bacteria have yet to be identified, and oil-seep fluids tend to contain methane (Joye et al., 2004; Valentine et al., 2010). Smrzka et al. (2016) put forward the concept of combining rare earth elements and yttrium ($\Sigma\text{REE} + \text{Y}$) versus Mo/U ratios of seep carbonates to discern oil-seep from methane-seep deposits. Early diagenetic, fibrous cement was shown to feature higher contents of $\Sigma\text{REE} + \text{Y}$ and lower Mo/U ratios in oil-seep deposits than in methane-seep deposits, which is likely to mirror the presence of crude oil in the fluids. Similarly, the enrichment of light rare earth elements (LREEs) in fibrous cement of oil-seep carbonates has been suggested to be related to the presence of crude oil, which provided an additional source of LREEs to the pore water from which the cement precipitated (Smrzka et al., 2019).

The presence of an additional carbon source at oil seeps is likely to affect the composition of organic matter in oil-seep carbonates. Unlike methane, which can at best be preserved in inclusions (but see Blumenberg et al., 2018), crude oil can be preserved in modern and ancient carbonates (Smrzka et al., 2016). The total organic carbon contents, carbon to nitrogen (C/N) and sulfur to carbon ratios (S/C), as well as $\delta^{13}\text{C}$ values of organic matter may, thus, serve as a tool for discriminating oil and methane seepage. To test whether organic matter preserved in seep carbonates could serve as an archive of fluid composition, a series of carbonates collected from oil- and methane-seep environments from the northern GoM was selected for a comprehensive geochemical study.

2. Site characteristics and samples

Numerous hydrocarbon seeps have been discovered since the 1980s on the northern continental slope of the GoM (Roberts et al., 2010). The geological history of the GoM is conducive for hydrocarbon seepage from deeply buried petroleum systems to the seafloor. Salt diapirism generated fault networks that provide conduits for gas, oil, and other fluids from deep reservoirs to surficial sediments (Roberts et al., 2010).

Table 1

Dive information, geographical coordinates, water depth, and bottom water temperature of sites GC232 and GC852 where carbonates were collected.

Sites	Year-dive number	Lat. Mean	Lon. Mean	Water depth (m)	Temperature (°C)
GC232					
	1991-JSL-3151	N27.7417°	W91.3188°	570	7.5
	1992-JSL-3302				
	1992-JSL-3304				
	1992-JSL-4401				
	1993-JSL-3564				
	1995-JSL-2636				
	1995-JSL-2369				
	2002-JSL-4401				
	2002-JSL-4403				
GC852					
	2006-Alvin-4177	N27.1060°	W91.1662°	1450	4.5
	2006-Jason-4185				
	2006-Alvin-4187				
	2007-Jason-273				
	2007-Jason-278				

Green Canyon (GC) is located on the upper slope of the GoM characterized by numerous gas and crude oil hydrocarbon seeps. Green Canyon block 232 (hereafter GC232) is situated at 570 m water depth, where the average bottom water temperature is ~7.5 °C (Fig. 1; Table 1). Geophysical data indicate that faults provide conduits for fluids and gas migration (Hackworth, 2005). The sediment contains abundant hydrogen sulfide (H_2S) and oil is visible infilling fractures in the sediment. Tubeworms and microbial mats lining fractures were present on the seafloor. Green Canyon block 852 (hereafter GC852) lies on the southern part of a steep-sided, N-S trending and elongated mound rising from a water depth of approximately 1450 m where the bottom water temperature is around 4.5 °C (Fig. 1; Table 1). More information on this active seepage site and its chemosynthesis-based communities is provided elsewhere (Roberts et al., 2010).

The carbonate samples studied herein were collected from the seafloor or the subsurface (< 50 cm below the seafloor) during nine *Johnson Sea Link* dives between 1992 and 2002, three deep submergence vehicle (DSV) *Alvin* dives in 2006, and two remotely operating vehicle (ROV) *Jason* dives in 2007 (Table 1). For the purpose of this study, samples from oil-dominated (site GC232) and methane-dominated (site GC852) seeps were selected for comparison. No apparent, systematic differences in the rock fabric between the authigenic carbonates from methane seeps and oil seeps have been recognized (Fig. 2). The carbonates come in a variety of shapes, including nodules, slabs, blocks, and irregularly shaped aggregates. Crude oil, which is apparently biodegraded, was found embedded in the samples from site GC232.

3. Analytical methods

The carbonate samples were washed with fresh water after

collection and subsequently air-dried. Bulk samples were selected to be ground into powder and then were separated for the subsequent analyses. Subsamples for carbonate carbon and oxygen stable isotopes were selected to reflect all stages of carbonate formation. For example, the microcrystalline matrix usually represents initial seepage-related precipitation, whereas cavity-filling cement typically reflects a later stage (Feng et al., 2010).

3.1. Carbonates carbon and oxygen stable isotopes

The powdered samples for $\delta^{13}C$ and $\delta^{18}O$ determination were obtained from rocks with a microdrill. Then samples were processed with 100% phosphoric acid at 90 °C to release CO_2 for analysis using a Thermo Finnigan Delta V Advantage mass spectrometer at Louisiana State University (LSU). The isotope values are reported using δ notation in per mil (‰) relative to the Vienna Pee Dee Belemnite (VPDB) standard. The analytical precision was on the order of 0.1‰ for both $\delta^{13}C$ and $\delta^{18}O$ values.

3.2. Major and trace elements

An aliquot of powdered samples was prepared for major and trace element analyses. Detailed measurement procedures followed the methods of Hu et al. (2014). The powdered samples were dissolved by a mixture of 1 ml HF (48%, v/v) and 1 ml HNO_3 (68%, v/v) in Teflon beakers. After dissolution in an electric oven at 185 °C for 36 h, the solution was then evaporated to dryness on a hot plate. After cooling, a mixture of 2 ml HNO_3 (68%, v/v) and 3 ml deionized water was added. The beakers were placed again in an electric oven at 135 °C for 5 h to dissolve the residue. Major and trace elements were analyzed using a Varian Vista Pro ICP-AES and a PerkinElmer Sciex ELAN 6000 ICP-MS

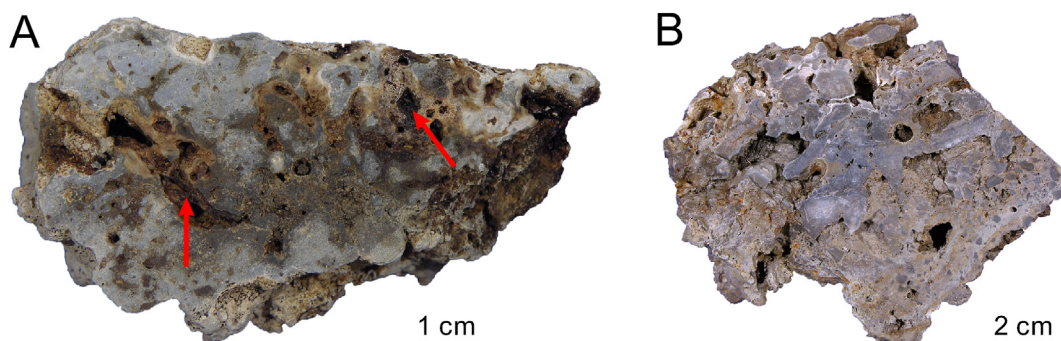


Fig. 2. Rock fabric of selected carbonate lithologies from sites GC232 (oil-seep) and GC852 (methane-seep). (A) Slab of carbonate collected from site GC232 with oil impregnations (arrows). (B) Carbonate sample from site GC852 revealing a porous fabric with carbonate clasts cemented by a micritic matrix.

at the Institute of Geochemistry, Chinese Academy of Sciences (CAS). Certified reference materials (GSR-1, OU-6, 1633-a, GXR-2, GXR-5) were used for quality control. Precision and accuracy were better than 5% for major elements and 10% for trace elements.

3.3. TOS, $\delta^{34}\text{S}_{\text{TOS}}$, and $\delta^{34}\text{S}_{\text{CRS}}$

About 2–5 g of the power sample was dissolved using 6 N HCl at 50 °C for 6 h to release acid volatile sulfur under a continuous flow of N₂ (g). Then the residue was analyzed for chromium reducible sulfur (CRS) by a modified version of the chromium reduction method (Li et al., 2016). The H₂S evolved was delivered into an AgNO₃ solution using continuous N₂ (g) and converted into Ag₂S for isotopic analyses ($\delta^{34}\text{S}_{\text{CRS}}$). After CRS extraction, the residue was washed with deionized water (3 times) and then dried for total organic sulfur (TOS) and stable isotope analyses ($\delta^{34}\text{S}_{\text{TOS}}$; cf. Canfield et al., 1998; Werne et al., 2003). The recovered Ag₂S and residue after chromium extraction were placed in tin boats with V₂O₅ and converted to SO₂ at 980 °C with an Elemental Analyzer. The analyses were conducted on an Isoprime100-EA with a peripheral elemental analyzer for on-line sample combustion at LSU. Precision and accuracy of the TOS were better than 5%. The standard deviation for $\delta^{34}\text{S}$ analysis was $\pm 0.3\text{\textperthousand}$, and the results were expressed using δ notation relative to the Vienna Canyon Diablo Troilite (VCDT) standard.

3.4. TOC, TN, and $\delta^{13}\text{C}_{\text{TOC}}$

Sub-samples of the samples above were digested with 0.5 N HCl for 24 h to eliminate carbonate. The residue was encapsulated with tin capsules and then measured for carbon isotope compositions ($\delta^{13}\text{C}_{\text{TOC}}$), as well as carbon and nitrogen contents (TOC, TN) following the method reported by Kumitsu et al. (2009). TOC, TN contents, and $\delta^{13}\text{C}_{\text{TOC}}$ measurements were performed in continuous-flow mode via an Elemental Analyzer interfaced to an Isoprime100 at LSU. The precision and accuracy of TOC and TN measurements were better than 5%. The $\delta^{13}\text{C}_{\text{TOC}}$ values are reported relative to VPDB. The precision for $\delta^{13}\text{C}_{\text{TOC}}$ is $\pm 0.2\text{\textperthousand}$.

4. Results

4.1. $\delta^{13}\text{C}_{\text{carb}}$ and $\delta^{18}\text{O}_{\text{carb}}$

The $\delta^{13}\text{C}$ values of carbonates from both sites show a large variation (Fig. 3; Table 2), from $-54.6\text{\textperthousand}$ to $-41.1\text{\textperthousand}$ (mean = $-49.5\text{\textperthousand}$, n = 12) for samples from site GC852 (methane seepage) and from $-27.2\text{\textperthousand}$ to $-11.8\text{\textperthousand}$ (mean = $-20.0\text{\textperthousand}$, n = 12) for samples from site GC232 (oil seepage). In contrast, $\delta^{18}\text{O}_{\text{carb}}$ values of all samples from both sites are very similar, ranging from $3.8\text{\textperthousand}$ to $5.2\text{\textperthousand}$ for site GC852 and from $3.6\text{\textperthousand}$ to $5.2\text{\textperthousand}$ for site GC232.

4.2. Major and trace elements

Selected major and trace elements contents for bulk carbonates are listed in Table 3. The Sr/Ca and Mg/Ca ratios of carbonates display a large variation between the two sites. Samples from site GC852 tend to have relatively higher Mg/Ca ratios, while carbonates from site GC232 reveal higher Sr/Ca ratios, pointing to predominant high-magnesium calcite (HMC) and aragonite composition, respectively (Fig. 4).

4.3. $\delta^{34}\text{S}_{\text{CRS}}$, $\delta^{34}\text{S}_{\text{TOS}}$, and TOS/TOC

Carbonates from site GC232 yielded more negative $\delta^{34}\text{S}_{\text{CRS}}$ and $\delta^{34}\text{S}_{\text{TOS}}$ values than rocks from site GC852 (Fig. 5). The $\delta^{34}\text{S}_{\text{TOS}}$ values of samples are higher than the corresponding $\delta^{34}\text{S}_{\text{CRS}}$ values of samples from both sites. Moreover, the $\delta^{34}\text{S}_{\text{CRS}}$ values co-vary with the $\delta^{34}\text{S}_{\text{TOS}}$ values of samples from both sites, except three samples (GC852-5,

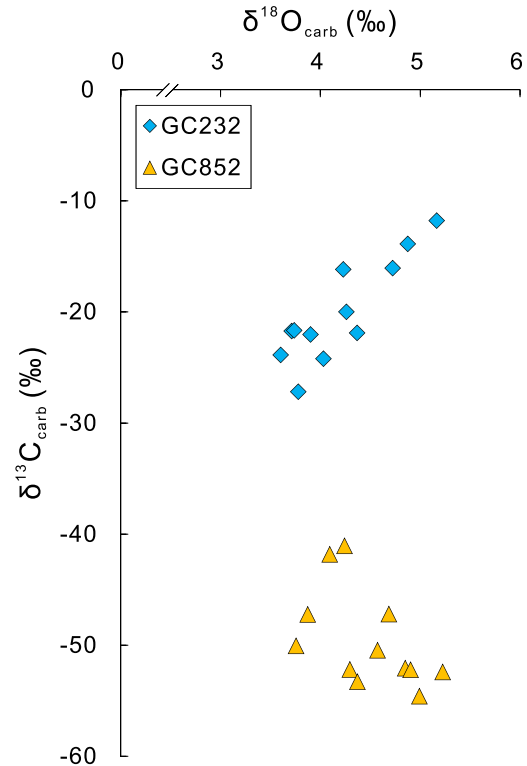


Fig. 3. Plot of $\delta^{13}\text{C}$ and $\delta^{18}\text{O}$ values of carbonates.

GC852-7, GC852-11; Fig. 5). Compared to rocks from site GC852, rocks from site GC232 reveal the higher TOS/TOC molar ratios and a wider variation of TOS/TOC ratios, ranging from 0.0054 to 0.0163 (Fig. 6). In addition, samples from site GC232 exhibit a positive correlation ($R^2 = 0.7$, n = 12) between the TOS/TOC ratio and TOC. Such correlation is not observed for samples from site GC852 (Fig. 6).

4.4. TOC, TN, and $\delta^{13}\text{C}_{\text{TOC}}$

TOC contents in samples from site GC232 are higher than those from site GC852, ranging from 0.17% to 1.09% (mean = 0.61%, n = 12), and from 0.17% to 0.32% (mean = 0.23%, n = 12), respectively. Carbonates from site GC232 yield higher TOC/TN weight ratios than carbonates from site GC852 (Table 2; Fig. 7). TOC/TN ratios range from 8.0 to 18.6 (mean = 12.3, n = 12) and 6.9 to 13.1 (mean = 12, n = 12) for samples from site GC232 and site GC852, respectively. The $\delta^{13}\text{C}_{\text{TOC}}$ values of carbonates from site GC852 fall between -68.7 and $-29.5\text{\textperthousand}$ (mean = $-45.4\text{\textperthousand}$, n = 12), while $\delta^{13}\text{C}_{\text{TOC}}$ values of carbonates from site GC232 are less negative, ranging from -45.4 to $-27.1\text{\textperthousand}$ (mean = $-35.7\text{\textperthousand}$, n = 12). Samples from both sites exhibit a positive correlation between the TOC/TN ratios and $\delta^{13}\text{C}_{\text{TOC}}$ values ($R^2 = 0.9$, n = 12 at site GC852, and $R^2 = 0.6$, n = 12 at site GC232; Fig. 7).

5. Discussion

5.1. Constraints on the environment of carbonate formation

The $\delta^{13}\text{C}_{\text{carb}}$ and $\delta^{34}\text{S}_{\text{CRS}}$ values as well as the mineralogy of seep carbonates are instrumental in deciphering the compositions of seepage fluids and carbonate formation environments (e.g., Peckmann and Thiel, 2004; Han et al., 2008, 2013; Feng et al., 2009). As expected for an oil-seep deposit, carbonates from site GC232 exhibit only moderately negative $\delta^{13}\text{C}$ values ($-27.2\text{\textperthousand}$ to $-11.8\text{\textperthousand}$). Such values, similar to values of oil from the Green Canyon reservoir ($\sim -27\text{\textperthousand}$; Kennicutt et al., 1988), suggest that the main carbon source for carbonate

Table 2

Carbon and oxygen stable isotopic compositions of carbonate, bulk geochemical parameters of residue after HCl dissolution and after chromium reduction, sulfur isotopic compositions of chromium reducible sulfur in carbonates. TOC = total organic carbon; TN = total nitrogen; TOS = total organic sulfur; CRS = chromium reducible sulfur.

Sites	Sample ID	carbonate		residue after HCl dissolution			residue after Cr ²⁺ reduction		Cr ²⁺ reducible sulfur	TOC/TN wt/wt	TOS/TOC mol/mol
		$\delta^{13}\text{C}_{\text{carb}}$	$\delta^{18}\text{O}_{\text{carb}}$	TOC	TN	$\delta^{13}\text{C}_{\text{TOC}}$	TOS	$\delta^{34}\text{S}_{\text{TOS}}$			
		%o, VPDB	%o, VPDB	wt%	wt%	%o, VPDB	µg/g	%o, VCDT			
GC232	GC232-1	-11.8	5.2	0.17	0.01	-27.1	34	2.9	-0.1	12.3	0.0076
	GC232-2	-16.2	4.2	0.61	0.05	-34.7	214	4.4	-8.7	12.0	0.0132
	GC232-3	-16.1	4.7	0.54	0.06	-39.5	189	6.2	-8.0	9.2	0.0131
	GC232-4	-20.0	4.3	0.75	0.06	-35.5	231	0.2	-9.1	13.6	0.0116
	GC232-5	-21.9	4.4	0.37	0.04	-38.0	53	2.9	-30.0	10.2	0.0054
	GC232-6	-24.2	4.0	0.40	0.05	-45.4	102	-0.4	-31.6	8.0	0.0096
	GC232-7	-27.2	3.8	0.79	0.07	-7.9	253	-3.9	-26.0	12.1	0.0120
	GC232-8	-21.7	3.7	1.09	0.06	-31.7	475	-3.1	-21.8	18.6	0.0163
	GC232-9	-13.9	4.9	0.58	0.03	-28.2	162	6.2	-13.8	17.2	0.0105
	GC232-10	-22.0	3.9	0.45	0.05	-40.4	96	0.7	-24.7	8.9	0.0080
	GC232-11	-23.9	3.6	0.86	0.06	-34.0	285	0.9	-23.6	13.7	0.0124
	GC232-12	-21.7	3.7	0.66	0.06	-35.4	179	-0.1	-11.5	11.5	0.0102
GC852	GC852-1	-41.8	4.1	0.19	0.01	-30.8	26	5.5	n.d.	13.1	0.0051
	GC852-2	-52.1	4.9	0.17	0.01	-29.5	22	3.8	-2.3	12.9	0.0049
	GC852-3	-52.2	4.9	0.27	0.03	-32.3	34	7.9	10.3	10.5	0.0048
	GC852-4	-54.6	5.0	0.27	0.02	-39.0	42	5.8	7.4	11.3	0.0059
	GC852-5	-50.1	3.8	0.32	0.04	-58.3	37	10.4	13.6	7.4	0.0044
	GC852-6	-47.2	3.9	0.27	0.04	-60.6	30	11.4	11.4	7.3	0.0041
	GC852-7	-52.2	4.3	0.26	0.02	-41.0	31	9.7	25.3	10.8	0.0044
	GC852-8	-52.4	5.2	0.22	0.03	-65.0	40	11.7	16.8	7.3	0.0069
	GC852-9	-47.2	4.7	0.17	0.02	-44.2	n.d.	n.d.	n.d.	10.4	n.d.
	GC852-10	-50.5	4.6	0.21	0.03	-68.7	23	9.7	-3.8	6.9	0.0042
	GC852-11	-53.3	4.4	0.28	0.02	-42.1	40	9.5	16.9	11.3	0.0053
	GC852-12	-41.1	4.2	0.18	0.02	-33.4	n.d.	n.d.	n.d.	11.1	n.d.

n.d. = not determined.

precipitation is biodegradation of heavy hydrocarbons and other oil-derived compounds (cf. Joye et al., 2004; Naehr et al., 2009). This interpretation is in line with the occurrence of oil-staining and unresolved complex mixtures of hydrocarbon compounds in carbonates from the same site (Woolsey et al., 2004, Fig. 2). Moreover, seep carbonates predominantly consisting of oil-derived carbon in other regions generally exhibit $\delta^{13}\text{C}$ values higher than -30o (Feng et al., 2008, 2009;

Naehr et al., 2009; Roberts et al., 2010; Mansour and Sassen, 2011; Mansour, 2014; Smrzka et al., 2019). Moreover, moderately negative carbon isotope values may also reflect thermogenic gas in addition to petroleum degradation, representing an alternative dissolved inorganic carbon source (e.g., Matturro et al., 2017; Oppo et al., 2017).

The extremely negative $\delta^{13}\text{C}$ values of carbonates from site GC852 (as low as -68.7o ; Fig. 3), on the other hand, point to biogenic

Table 3

Calculated carbonate contents and selected major element compositions in the studied carbonates.

Sites	Sample ID	CaO	MgO	^a CaCO ₃	Sr	Ba	Al	Mg/Ca	Sr/Ca
		wt%	wt%	wt%	µg/g	µg/g	wt%	g/g	g/g
GC232	GC232-1	37.4	7.6	82.7	942	299	1.39	0.122	0.003
	GC232-2	42.2	3.9	83.4	5120	335	1.02	0.055	0.013
	GC232-3	43.2	3.0	83.3	6530	367	0.92	0.041	0.017
	GC232-4	41.1	4.8	83.5	4620	93	0.97	0.071	0.012
	GC232-5	39.2	5.9	82.4	2010	103	1.35	0.090	0.006
	GC232-6	44.2	2.3	83.9	5920	68	0.85	0.032	0.015
	GC232-7	43.1	2.0	81.1	8280	78	1.12	0.028	0.016
	GC232-8	42.8	2.4	81.4	6790	65	0.98	0.033	0.018
	GC232-9	31.7	11.3	80.4	6180	68	1.74	0.213	0.022
	GC232-11	45.5	0.8	83.0	7310	134	0.95	0.011	0.018
	GC232-12	42.8	2.8	82.2	5810	68	1.01	0.039	0.015
	GC852-1	38.7	5.2	80.0	811	315	1.65	0.080	0.003
GC852	GC852-2	37.0	7.2	81.1	685	107	1.45	0.117	0.003
	GC852-3	33.1	8.9	77.8	769	239	1.95	0.161	0.003
	GC852-4	34.3	7.8	77.6	756	142	1.82	0.136	0.003
	GC852-5	43.2	1.3	79.9	6900	85	1.15	0.018	0.018
	GC852-6	42.8	2.2	81.0	7210	85	1.12	0.031	0.019
	GC852-7	35.9	7.6	80.1	1330	122	1.60	0.128	0.005
	GC852-8	39.1	6.4	83.3	3530	97	1.21	0.099	0.010
	GC852-9	40.7	1.9	76.8	6240	115	1.57	0.029	0.017
	GC852-10	42.8	3.2	83.1	7430	68	0.91	0.045	0.020
	GC852-11	34.6	7.2	76.8	1010	249	1.75	0.124	0.004
	GC852-12	38.6	5.2	79.9	780	304	1.66	0.081	0.003

^a CaCO₃ = CaCO₃ + MgCO₃.

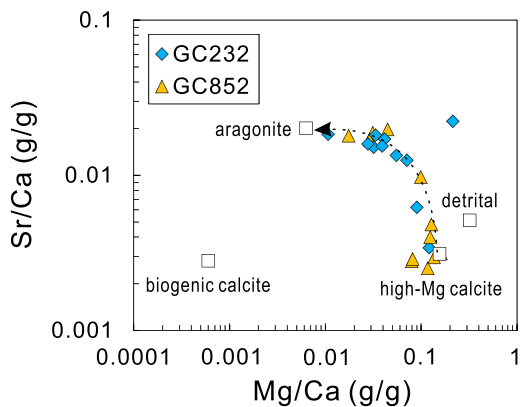


Fig. 4. Relationship between Sr/Ca and Mg/Ca ratios (wt%). The dashed line corresponds to mixing lines between hypothetical end-members of high-Mg calcite and aragonite. End members of Sr/Ca and Mg/Ca ratios from Gong et al. (2018). Data from Bayon et al. (2007) were used for biogenic calcites. The Sr/Ca and Mg/Ca ratios of detrital fraction were calculated from Pickering and Stow (1986).

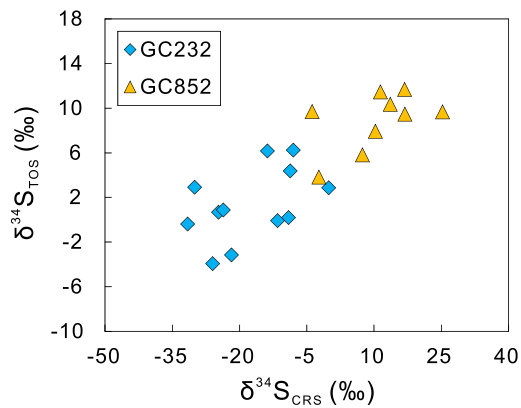


Fig. 5. Plots of $\delta^{34}\text{S}_{\text{CRS}}$ and $\delta^{34}\text{S}_{\text{org}}$ values of carbonate samples.

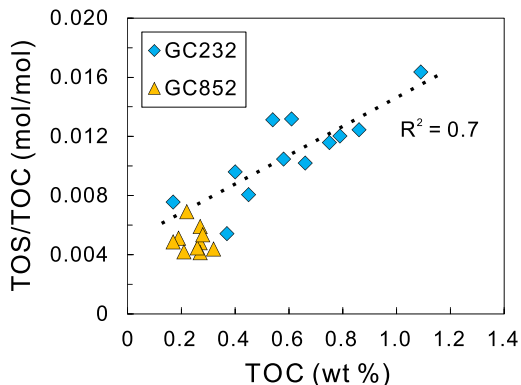


Fig. 6. Relationships between content of organic sulfur and total organic carbon (TOS/TOC; molar ratios) and total organic carbon (TOC, wt%) of the residue of carbonate samples after chromium reduction.

methane as main carbon source. This interpretation is supported by the carbon isotopic composition of GC852 methane ($-75\text{\textperthousand}$; Joye et al., 2010) and the presence of extremely ¹³C-depleted archaeal lipids (Guan et al., 2019). It should, however, be stressed that the substantial offset in $\delta^{13}\text{C}$ values between carbonates from oil and methane seeps found in this study is not necessarily typifying the different modes of seepage. Samples from both sites display similar $\delta^{18}\text{O}_{\text{carb}}$ values (Fig. 3). Assuming the carbonate precipitated from present bottom water at current seawater temperature (Table 1) and a $\delta^{18}\text{O}_{\text{seawater}}$ value of $0.7\text{\textperthousand}$ SMOW

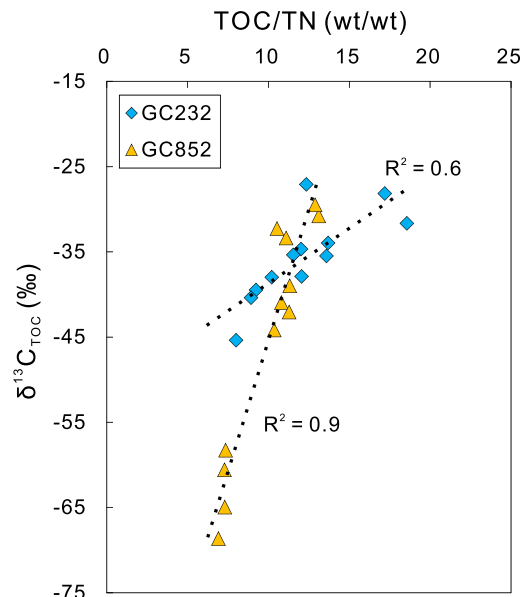


Fig. 7. Relationship between the $\delta^{13}\text{C}$ values of total organic carbon and total organic carbon/nitrogen (TOC/TN) weight ratios of bulk carbonate samples.

(Feng et al., 2008), the equilibrium $\delta^{18}\text{O}_{\text{carb}}$ values of aragonite and HMC can be calculated (Kim and O’Neil, 1997; Kim et al., 2007). The calculated $\delta^{18}\text{O}$ values are $+2.9\text{\textperthousand}$ for aragonite for site GC232 and $+2.8\text{\textperthousand}$ for HMC from site GC852. The majority of the measured $\delta^{18}\text{O}$ values are higher than these calculated values, which points to the involvement of ¹⁸O-enriched fluids during carbonate formation. Thus, the values probably reflect destabilization of gas hydrate, which is particularly abundant at the two study sites (Orcutt et al., 2005).

Based on the concept of Bayon et al. (2007), Sr/Ca vs. Mg/Ca ratios suggest that samples from GC232 are dominated by aragonite, while high-magnesium calcite (HMC) is the main carbonate mineral of rocks from site GC852 (Fig. 4). It has been suggested that the presence of dissolved sulfate inhibits both calcite and aragonite precipitation, but inhibition is more pronounced for calcite (Mucci et al., 1989). Alternatively, high sulfide concentrations, resulting from AOM at seeps, may catalyze calcite formation (Lu et al., 2018). Irrespective of the dominant mechanism, aragonite will be favored in high sulfate/low sulfide environments close to the seafloor, whereas formation of HMC will preferentially occur at greater depth in low sulfate/high sulfide environments (Burton, 1993; Savard et al., 1996; Haas et al., 2010). Accordingly, the formation of GC852 calcite probably took place deeper within the sediment, while the formation of GC232 aragonite occurred closer to the seafloor. Interestingly, the dominance of aragonite in oil-seep deposits has been observed before (Peckmann et al., 2007; Feng et al., 2009; Naehr et al., 2009; Mansour and Sassen, 2011; Mansour, 2014; Smrzka et al., 2019). Because it is refractory, crude oil tends to migrate to shallower depth, as supported by massive oil deposits observed on the seafloor (MacDonald et al., 2004; Naehr et al., 2009). Moreover, the anaerobic oxidation of crude oil components comes along with low rates of microbial sulfate reduction (Aharon and Fu, 2000). The slow consumption of sulfate renders the more enriched residual sulfate in pore water (Mansour, 2014). Hence, oil degradation at shallow depth and relatively low sulfate reduction rates favor fast replenishment of the pool of dissolved sulfate at oil seeps and aragonite formation. At methane seeps, mineralogy of authigenic carbonates is chiefly controlled by seepage intensity (Luff and Wallmann, 2003; Peckmann et al., 2009).

The envisioned formation conditions of carbonates from the two study sites also agree with sulfur isotope signatures of CRS (Gong et al., 2018; Tong et al., 2019). The markedly negative $\delta^{34}\text{S}_{\text{CRS}}$ values of GC232 samples point to carbonate precipitation close to the seafloor. In

contrast, $\delta^{34}\text{S}$ -enriched CRS from carbonates of site GC852 indicates formation at greater depth. Two main mechanisms controlling $\delta^{34}\text{S}$ values of the released hydrogen sulfide during microbial sulfate reduction are (1) the sulfur isotopic fractionation of sulfate reduction and (2) the sulfur isotopic composition of sulfate in the pore water pool (Gong et al., 2018). Pronounced $\delta^{34}\text{S}$ -depletion in CRS at site GC232 is attributed to fast replenishment of dissolved sulfate and a potential effect of sulfur re-oxidative cycling. Another factor that contributes to the sulfur isotope pattern is sulfate reduction rate. CRS formed in oil-seep environments has low $\delta^{34}\text{S}$ values since crude oil is more refractory than the smaller methane molecule, which leads to lower sulfate reduction rates and larger sulfur isotope fractionation associated with sulfate reduction at oil seeps than at methane seeps (Aharon and Fu, 2000). Sulfide minerals with high $\delta^{34}\text{S}$ values, on the other hand, reflect formation at greater depth, where the environment is more restricted for sulfate, resulting in a $\delta^{34}\text{S}$ -enriched pool of residual sulfate (Peketi et al., 2015; Li et al., 2016; Gong et al., 2018; Tong et al., 2019). The $\delta^{34}\text{S}_{\text{CRS}}$ values are consequently consistent with the conclusions derived from the predominant mineralogies of the samples from the two study sites.

5.2. Signatures of organic matter in authigenic carbonates from oil and methane seeps

The determination of TOC, TN, and TOS contents, coupled with $\delta^{13}\text{C}_{\text{TOC}}$ values can be used to constrain sources of organic matter (Meyers, 1997; Lepot et al., 2019), which will be different for oil and methane seeps. The TOS/TOC ratios of rocks are controlled mainly by organic matter sulfurization and organic matter sources (cf. Werne et al., 2008). In this study, organic matter from carbonates of the methane-seep site GC852 shows lower TOS/TOC ratios than carbonates of the oil-seep site GC232 (Fig. 6). The covariation of the $\delta^{34}\text{S}_{\text{CRS}}$ and $\delta^{34}\text{S}_{\text{TOS}}$ values of samples from both sites (Fig. 5) likely indicates organic sulfur chiefly derived from diagenetic organic matter sulfurization (cf. Werne et al., 2008). A deeper formation depth of carbonates is in favor of the accumulation of dissolved sulfide in pore water (cf. Tong et al., 2019) and organic matter sulfurization (e.g., Quijada et al., 2016). Samples from site GC852 apparently precipitated at a greater depth based on $\delta^{34}\text{S}$ -enriched CRS and the dominance of HMC. Therefore, it is reasonable to attribute the higher TOS/TOC ratios of samples from site GC232 to the input of organic matter with a high TOS/TOC ratio, instead of enhanced organic matter sulfurization. Oil impregnation of GC232 rocks agrees with crude oil as the main cause for the high TOS/TOC ratios. Crude oil is characterized by a high organic sulfur content (Hughes et al., 1995; Hood et al., 2002; Smrzka et al., 2019). Kelemen et al. (2010) have shown that natural solid bitumen exhibits high levels of organic sulfur (S/C atomic ratios ~0.03 to 0.17). The linear correlation ($R^2 = 0.7$) between TOS/TOC ratios and TOC of samples from site GC232 also suggests local input of organic matter characterized by high TOS/TOC ratios (Fig. 6). The presence of crude oil at site GC232 is reflected in TOS and TOC enriched samples. Therefore, the leakage of crude oil at site GC232 is likely the main cause for the high TOS/TOC ratios and the covariation between TOS/TOC ratios and TOC of samples.

The $\delta^{13}\text{C}_{\text{TOC}}$ values along with TOC/TN ratios of organic matter provide information on carbon sources (Paull et al., 1992). The $\delta^{13}\text{C}_{\text{TOC}}$ values obtained for GC232 and GC852 samples are lower than average background values of organic matter in the GoM (~21.7‰ to ~19.7‰; Goñi et al., 1998). Thus, a local origin related to hydrocarbon seepage is apparent. Positive correlation between $\delta^{13}\text{C}_{\text{TOC}}$ and TOC/TN ratios ($R^2 = 0.9$ for site GC852 and $R^2 = 0.6$ for site GC232) in the samples may suggest binary mixing of two sources of organic matter (Fig. 7). For the samples from site GC852, one end-member shows very low $\delta^{13}\text{C}_{\text{TOC}}$ values and low TOC/TN ratios, the other one is characterized by higher $\delta^{13}\text{C}_{\text{TOC}}$ values and TOC/TN ratios. The $\delta^{13}\text{C}_{\text{TOC}}$ value is as low as ~68.7‰, close to the $\delta^{13}\text{C}$ value of methane from site

GC852 (~75‰; Joye et al., 2010), which is consistent with the local presence of ^{13}C -depleted lipids of methanotrophic archaea (Guan et al., 2019). Such ^{13}C -depletion of sedimentary organic matter is caused by the assimilation of methane (e.g., Paull et al., 1992; Williscroft et al., 2017), probably reflecting to a large extent the buried biomass of AOM consortia in case of site GC852 (Guan et al., 2019). This interpretation is supported by low TOC/TN ratios (as low as 6.9; Fig. 7) of samples showing markedly negative $\delta^{13}\text{C}_{\text{TOC}}$ values, since microbial residue usually exhibits low C/N ratios ranging from 4 to 6 (Meyers, 1997). Similarly, Paull et al. (1992) have suggested that seep synthesized organic matter is the reason for low C/N ratios (< 7.5) of organic matter in seep sediments. Contrary to this, organic matter from GoM background sediments displays C/N ratios of ~11 (Goñi et al., 1998).

Organic matter extracted from sediment affected by oil is typified by high C/N ratios (Joye et al., 2004; Lamontagne et al., 2004; Hackworth, 2005; Rumolo et al., 2011; Bowles et al., 2016). For instance, Wang et al. (2001) reported high C/N ratios (17–28) of organic matter from sediment containing petroleum hydrocarbons from the northern GoM. Previous studies have shown that $\delta^{13}\text{C}_{\text{TOC}}$ values of oil-seep carbonates and sediments match well with $\delta^{13}\text{C}$ values of the corresponding reservoir oils (e.g., Kennicutt et al., 1988; Wang et al., 2001). The offset between $\delta^{13}\text{C}$ values of oil from the Green Canyon reservoir (~−27‰, Kennicutt et al., 1988) and the $\delta^{13}\text{C}_{\text{TOC}}$ values of samples from site GC232 consequently suggests a contribution from another source characterized by low TOC/TN ratios and ^{13}C -depletion. Such additional source could be represented by the biomass of AOM consortia, as oil seeps generally contain some methane (Valentine et al., 2010) supporting AOM activity (Naehr et al., 2009). Moreover, the $\delta^{13}\text{C}_{\text{methane}}$ value reported for this site (~−43‰; Woolsey et al., 2004) is close to the most negative $\delta^{13}\text{C}_{\text{TOC}}$ value (~−45.4‰) observed in this study. On the other hand, microbial oil degradation can also result in ^{13}C -depleted carbon in organic residue fractions, with $\delta^{13}\text{C}$ values of ~−36.7‰ reported for GoM oil seeps (Anderson et al., 1983). Overall, our data confirm that C/N ratios along with $\delta^{13}\text{C}$ values of organic matter can provide robust information on the sources of organic matter enclosed in seep carbonates.

5.3. Identifying oil and methane seeps in the geological record

The ability to discern oil seeps from methane seeps is a precondition for understanding the adaptation of chemosynthesis-based life to oil seeps and carbon cycling at seeps through geological time (Smrzka et al., 2016, 2019; Kiel and Peckmann, 2019). Approaches have been developed to identify past oil seepage using carbon isotope compositions and trace element patterns (REEs, Mo and U) of seep carbonates (Peckmann et al., 2007; Smrzka et al., 2016, 2019). Carbon stable isotope compositions of seep carbonates are not sufficient to confirm oil-driven carbonate formation due to the unknown degree of mixing between different carbon sources (Peckmann and Thiel, 2004). Oil seep environments provide suitable conditions for aragonite precipitation as revealed in this study. On the other hand, we need to caution that aragonite also forms at methane seeps when flux is high (e.g., Luff and Wallmann, 2003). However, fibrous aragonite cement of oil-seep deposits has been shown to be enriched in REEs and to exhibit systematically lower Mo/U ratios than its counterpart from methane-seep deposits (Smrzka et al., 2016, 2019). Moreover, the presence of crude oil tends to cause an enrichment of LREEs in aragonite at modern seeps (Smrzka et al., 2019). The new data on GC232 and GC852 presented here reveal that TOS/TOC ratios and $\delta^{13}\text{C}_{\text{TOC}}$ – TOC/TN patterns also allow identification of carbonates forming at oil seeps. This new approach complements the trace element (Mo and U) and REE proxy in identifying oil-seep deposits in the geological record. The new approach is particularly promising for seep limestones dominated by a micro-crystalline carbonate matrix and lacking abundant fibrous cement. It will, however, be compromised in cases of substantial diagenetic alteration and high thermal maturity. At hydrocarbon seeps, high

amounts of hydrogen sulfide produced by microbial sulfate reduction can result in pronounced organic matter sulfurization (Quijada et al., 2016). It has been shown that sulfurization can enhance preservation of organic matter (e.g., Werne et al., 2008). In addition, high rates of carbonate precipitation can result in efficient preservation of organic matter in seep deposits (Peckmann and Thiel, 2004). For example, organic matter with extreme ^{13}C -depletion ($-65.2\text{\textperthousand}$) preserved in Neoarchean rocks is likely to reflect organic matter sulfurization (Lepot et al., 2019). Therefore, well-preserved organic matter enclosed in authigenic carbonate may serve as an archive of the different types of hydrocarbon seepage (i.e., methane seeps and oil seeps). However, it should be stressed that possible transitions between oil and methane dominance at a seep site may also affect the analyzed geochemical parameters. Oil seeps can be constrained with the aid of the higher TOS/TOC and TOC/TN ratios. However, the presence of methane seepage may be overlooked, since oil seeps always contain some methane (Valentine et al., 2010). Our study provides new means to identify hydrocarbon sources of ancient chemosynthesis-based ecosystems, facilitating the discrimination of former oil seeps from methane seeps.

6. Conclusions

This comparative study of authigenic carbonates from Gulf of Mexico (GoM) oil and methane seeps, using mineral compositions as well as sulfur stable isotopes of chromium reducible sulfur (CRS) and organic sulfur, indicates that microbial degradation of crude oil results in carbonate precipitation close to the seafloor at an oil-seep site. A strong linear covariation of TOS/TOC ratios and TOC of carbonates from an oil seep suggests the contribution of crude oil to the pool of organic matter preserved in oil-seep carbonates. The oil-seep deposit reveals higher TOC/TN ratios and $\delta^{13}\text{C}_{\text{TOC}}$ values than the methane-seep deposit. Similarly, TOS/TOC and $\delta^{13}\text{C}_{\text{TOC}} - \text{TOC/TN}$ patterns of organic matter enclosed in seep carbonates can help identifying the carbon sources during carbonate authigenesis. These results suggest that organic matter contained in seep limestones may provide information of fluid composition. Provided that such organic matter is well preserved, not having been altered in the course of diagenesis, the new approach has potential to constrain the composition of hydrocarbon components of ancient seepage systems.

CRediT authorship contribution statement

Yuedong Sun: Formal analysis, Writing - review & editing. **Shanggui Gong:** Methodology, Writing - review & editing, Formal analysis, Writing - original draft. **Niu Li:** Formal analysis, Writing - review & editing. **Jörn Peckmann:** Writing - review & editing. **Meng Jin:** Formal analysis, Writing - review & editing. **Harry H. Roberts:** Data curation, Writing - review & editing. **Duofu Chen:** Writing - review & editing. **Dong Feng:** Methodology, Writing - review & editing, Data curation.

Acknowledgments

Samples were collected during projects funded by the U.S. Bureau of Ocean Energy Management and the National Oceanic and Atmospheric Administration's National Undersea Research Program. We are grateful to Y.B. Peng (LSU) for stable isotope measurements. This study was partially supported by the NSF of China (Grants: 41761134084, 41773091 and 41730528), the National Program on Global Change and Air-Sea Interaction (GASI-GEOGE-05-04) and the Deutsche Forschungsgemeinschaft (PE 847/7-1). Yuedong Sun acknowledges the China Scholarship Council for supporting a research visit to Universität Hamburg. This article benefited from insightful comments of Associate Editor Dr. Davide Oppo and two anonymous reviewers.

Appendix A. Supplementary data

Supplementary data to this article can be found online at <https://doi.org/10.1016/j.marpgeo.2020.104230>.

References

- Agirrezabal, L.M., 2009. Mid-Cretaceous hydrothermal vents and authigenic carbonates in a transform margin, Basque-Cantabrian Basin (western Pyrenees): a multidisciplinary study. *Sedimentology* 56, 969–996.
- Aharon, P., Fu, B., 2000. Microbial sulfate reduction rates and sulfur and oxygen isotope fractionations at oil and gas seeps in deepwater Gulf of Mexico. *Geochim. Cosmochim. Acta* 64, 233–246.
- Anderson, R.K., Scalan, R.S., Parker, P.L., Behrens, E.W., 1983. Seep oil and gas in Gulf of Mexico slope sediment. *Science* 222, 619–621.
- Bayon, G., Pierre, C., Etoubleau, J., Voisset, M., Cauquil, E., Marsset, T., Sultan, N., Le Drezén, E., Fouquet, Y., 2007. Sr/Ca and Mg/Ca ratios in Niger Delta sediments: implications for authigenic carbonate genesis in cold seep environments. *Mar. Geol.* 241, 93–109.
- Blumenberg, M., Pape, T., Seifert, R., Bohrmann, G., Schlömer, S., 2018. Can hydrocarbons entrapped in seep carbonates serve as gas geochemistry recorder? *Geo Mar. Lett.* 38, 121–129.
- Bowles, M., Hunter, K.S., Samarkin, V., Joye, S., 2016. Patterns and variability in geochemical signatures and microbial activity within and between diverse cold seep habitats along the lower continental slope, Northern Gulf of Mexico. *Deep-Sea Res. Part II: Top. Stud. in Oceanogr.* 129, 31–40.
- Burton, E.A., 1993. Controls on marine carbonate cement mineralogy: review and reassessment. *Chem. Geol.* 105, 163–179.
- Campbell, K.A., 2006. Hydrocarbon seep and hydrothermal vent paleoenvironments and paleontology: past developments and future research directions. *Paleogeogr. Paleoclimatol. Paleoecol.* 232, 362–407.
- Canfield, D.E., Boudreau, B.P., Mucci, A., Gundersen, J.K., 1998. The early diagenetic formation of organic sulfur in the sediments of Mangrove Lake, Bermuda. *Geochim. Cosmochim. Acta* 62, 767–781.
- Ceramicola, S., Dupré, S., Somoza, L., Woodside, J., 2018. Cold seep systems. In: Micallef, A., Krastel, S., Savini, A. (Eds.), *Submarine Geomorphology*. Springer International Publishing, Cham, pp. 367–387.
- Feng, D., Chen, D., Qi, L., Roberts, H.H., 2008. Petrographic and geochemical characterization of seep carbonate from Alaminos Canyon, Gulf of Mexico. *Chin. Sci. Bull.* 53, 1716–1724.
- Feng, D., Chen, D., Roberts, H.H., 2009. Petrographic and geochemical characterization of seep carbonate from Bush Hill (GC 185) gas vent and hydrate site of the Gulf of Mexico. *Mar. Pet. Geol.* 26, 1190–1198.
- Feng, D., Roberts, H.H., Cheng, H., Peckmann, J., Bohrmann, G., Edwadrs, R.L., Chen, D., 2010. U/Th dating of cold-seep carbonates: an initial comparison. *Deep-Sea Res. Part II* 57, 2055–2060.
- Freire, A.F.M., Iemini, J.A., Viana, A.R., Magnavita, L.P., Dehler, N.M., Kowsmann, R.O., Miller, D.J., Bezerra, S.H.D.G., Zerfass, G.d.S.d.A., Shimabukuro, S., Nóbrega II, M., 2017. A giant oil seep at a salt-induced escarpment of the São Paulo Plateau, Espírito Santo Basin, off Brazil: host rock characteristics and geochemistry. *Deep-Sea Res. Part II: Top. Stud. in Oceanogr.* 146, 45–52.
- Gong, S., Hu, Y., Li, N., Feng, D., Liang, Q., Tong, H., Peng, Y., Tao, J., Chen, D., 2018. Environmental controls on sulfur isotopic compositions of sulfide minerals in seep carbonates from the South China Sea. *J. Asian Earth Sci.* 168, 96–105.
- Goñi, M.A., Ruttenberg, K.C., Eglington, T.I., 1998. A reassessment of the sources and importance of land-derived organic matter in surface sediments from the Gulf of Mexico. *Geochim. Cosmochim. Acta* 62, 3055–3075.
- Guan, H., Feng, D., Birgel, D., Peckmann, J., Roberts, H.H., Wu, N., Chen, D., 2019. Lipid biomarker patterns reflect different formation environments of mussel- and tube-worm-dominated seep carbonates from the Gulf of Mexico (Atwater Valley and Green Canyon). *Chem. Geol.* 505, 36–47.
- Haas, A., Peckmann, J., Elvert, M., Sahling, H., Bohrmann, G., 2010. Patterns of carbonate authigenesis at the Kouilou pockmarks on the Congo deep-sea fan. *Mar. Geol.* 268, 129–136.
- Hackworth, M.S., 2005. Carbonate Records of Submarine Hydrocarbon Venting: Northern Gulf of Mexico. LSU Doctoral Dissertations, pp. 2955.
- Han, X., Suess, E., Huang, Y., Wu, N., Bohrmann, G., Su, X., Eisenhauer, A., Rehder, G., Fang, Y., 2008. Jiulong methane reef: microbial mediation of seep carbonates in the South China Sea. *Mar. Geol.* 249, 243–256.
- Han, X., Yang, K., Huang, Y., 2013. Origin and nature of cold seep in northeastern Dongsha area, South China Sea: evidence from chimney-like seep carbonates. *Chin. Sci. Bull.* 58, 3689–3697.
- Hood, K.C., Wenger, L., Gross, O., Harrison, S., 2002. Hydrocarbon systems analysis of the northern Gulf of Mexico: delineation of hydrocarbon migration pathways using seeps and seismic imaging. *Surf. Explor. Case Hist.: Appl. Geochem. Magn. Remote Sens. AAPG Stud. Geol.* 48, 25–40.
- Hu, Y., Feng, D., Peckmann, J., Roberts, H.H., Chen, D.F., 2014. New insights into cerium anomalies and mechanisms of trace metal enrichment in authigenic carbonate from hydrocarbon seeps. *Chem. Geol.* 381, 55–66.
- Hughes, W.B., Holba, A.G., Dzou, L.I.P., 1995. The ratios of dibenzothiophene to phenanthrene and pristane to phytane as indicators of depositional environment and lithology of petroleum source rocks. *Geochim. Cosmochim. Acta* 59, 3581–3598.
- Joye, S.B., Boetius, A., Orcutt, B.N., Montoya, J.P., Schulz, H.N., Erickson, M.J., Lugo, S.K., 2004. The anaerobic oxidation of methane and sulfate reduction in sediments

- from Gulf of Mexico cold seeps. *Chem. Geol.* 205, 219–238.
- Joye, S.B., Bowles, M.W., Samarkin, V.A., Hunter, K.S., Niemann, H., 2010. Biogeochemical signatures and microbial activity of different cold-seep habitats along the Gulf of Mexico deep slope. *Deep-Sea Res. Part II: Top. Stud. in Oceanogr.* 57, 1990–2001.
- Kleemann, S.R., Walters, C.C., Kwiatek, P.J., Freund, H., Afeworki, M., Sansone, M., Lamberti, W.A., Pottorf, R.J., Machel, H.G., Peters, K.E., Bolin, T., 2010. Characterization of solid bitumens originating from thermal chemical alteration and thermochemical sulfate reduction. *Geochem. Cosmochim. Acta* 74, 5305–5332.
- Kennicutt, M.C., Brooks, J.M., Denoux, G.J., 1988. Leakage of deep, reservoired petroleum to the near surface on the gulf of Mexico Continental slope. *Mar. Chem.* 24, 39–59.
- Kiel, S., Peckmann, J., 2019. Resource partitioning among brachiopods and bivalves at ancient hydrocarbon seeps: a hypothesis. *PLoS One* 14, e0221887.
- Kim, S.T., O'Neil, J.R., 1997. Equilibrium and nonequilibrium oxygen isotope effects in synthetic carbonates. *Geochem. Cosmochim. Acta* 61, 3461–3475.
- Kim, S.T., O'Neil, J.R., Hillaire-Marcel, C., Mucci, A., 2007. Oxygen isotope fractionation between synthetic aragonite and water: influence of temperature and Mg^{2+} concentration. *Geochem. Cosmochim. Acta* 71, 4704–4715.
- Körber, J.H., Sahling, H., Pape, T., Ferreira, C.D.S., Macdonald, I., Bohrmann, G., 2014. Natural oil seepage at kobuleti ridge, eastern Black Sea. *Mar. Pet. Geol.* 50, 68–82.
- Kunimitsu, Y., Togo, T., Sampei, Y., Kano, A., Yasui, K., 2009. Organic compositions of the embryo-bearing lowermost Cambrian Kuanchuanpu formation on the northern Yangtze platform, China. *Paleogeogr. Paleoclimatol. Paleoccol.* 280, 499–506.
- Lamontagne, M.G., Ira, L., Sandra, B., Werfhorst, L.C., Van De, Holden, P.A., 2004. Bacterial diversity in marine hydrocarbon seep sediments. *Environ. Microbiol.* 6, 799–808.
- Leplat, K., Williford, K.H., Philippot, P., Thomazo, C., Ushikubo, T., Kitajima, K., Mostefaoui, S., Valley, J.W., 2019. Extreme ^{13}C -depletions and organic sulfur content argue for S-fueled anaerobic methane oxidation in 2.72 Ga old stromatolites. *Geochem. Cosmochim. Acta* 244, 522–547.
- Li, N., Feng, D., Chen, L., Wang, H., Chen, D., 2016. Using sediment geochemistry to infer temporal variation of methane flux at a cold seep in the South China Sea. *Mar. Pet. Geol.* 77, 835–845.
- Lu, Y., Sun, X., Xu, H., Konishi, H., Lin, Z., Xu, L., Chen, T., Hao, X., Lu, H., Peckmann, J., 2018. Formation of dolomite catalyzed by sulfate-driven anaerobic oxidation of methane: mineralogical and geochemical evidence from the northern South China Sea. *Am. Mineral.* 103, 720–734.
- Luff, R., Wallmann, K., 2003. Fluid flow, methane fluxes, carbonate precipitation and biogeochemical turnover in gas hydrate-bearing sediments at Hydrate Ridge, Cascadia Margin: numerical modeling and mass balances. *Geochem. Cosmochim. Acta* 67, 3403–3421.
- MacDonald, I.R., Bohrmann, G., Escobar, E., Abegg, F., Blanchon, P., Blinova, V., Brückmann, W., Drews, M., Eisenhauer, A., Han, X., 2004. Asphalt volcanism and chemosynthetic life in the Campeche Knolls, Gulf of Mexico. *Science* 304, 999–1002.
- Mansouri, A.S., 2014. Hydrocarbon-derived carbonates along the upper-lower continental slope, Gulf of Mexico: mineralogical and stable isotopic study. *Carbonates Evaporites* 29, 89–105.
- Mansouri, A.S., Sassen, R., 2011. Mineralogical and stable isotopic characterization of authigenic carbonate from a hydrocarbon seep site, Gulf of Mexico slope: possible relation to crude oil degradation. *Mar. Geol.* 281, 59–69.
- Matturro, B., Cruz Viggi, C., Aulenta, F., Rossetti, S., 2017. Cable bacteria and the bioelectrochemical snorkel: the natural and engineered facets playing a role in hydrocarbons degradation in marine sediments. *Front. Microbiol.* 8, 952.
- Mbadinga, S.M., Wang, L.-Y., Zhou, L., Liu, J.-F., Gu, J.-D., Mu, B.-Z., 2011. Microbial communities involved in anaerobic degradation of alkanes. *Int. Biodeterior. Biodegrad.* 65, 1–13.
- Meyers, P.A., 1997. Organic geochemical proxies of paleoceanographic, paleolimnologic, and paleoclimatic processes. *Org. Geochem.* 27, 213–250.
- Mucci, A., Canuel, R., Zhong, S., 1989. The solubility of calcite and aragonite in sulfate-free seawater and the seeded growth kinetics and composition of the precipitates at 25°C. *Chem. Geol.* 74, 309–320.
- Musat, F., 2015. The anaerobic degradation of gaseous, nonmethane alkanes - from in situ processes to microorganisms. *Comput. Struct. Biotechnol. J.* 13, 222–228.
- Naeher, T.H., Birgel, D., Bohrmann, G., MacDonald, I.R., Kasten, S., 2009. Biogeochemical controls on authigenic carbonate formation at the Chapopote "asphalt volcano", Bay of Campeche. *Chem. Geol.* 266, 390–402.
- Oppo, D., Viola, I., Capozzi, R., 2017. Fluid sources and stable isotope signatures in authigenic carbonates from the Northern Apennines, Italy. *Mar. Pet. Geol.* 86, 606–619.
- Orcutt, B., Boettius, A., Elvert, M., Samarkin, V., Joye, S.B., 2005. Molecular biogeochemistry of sulfate reduction, methanogenesis and the anaerobic oxidation of methane at Gulf of Mexico cold seeps. *Geochem. Cosmochim. Acta* 69, 4267–4281.
- Orcutt, B.N., Joye, S.B., Kleindienst, S., Knittel, K., Ramette, A., Reitz, A., Samarkin, V., Treude, T., Boettius, A., 2010. Impact of natural oil and higher hydrocarbons on microbial diversity, distribution, and activity in Gulf of Mexico cold-seep sediments. *Deep-Sea Res. Part II: Top. Stud. in Oceanogr.* 57, 2008–2021.
- Paull, C.K., Chanton, J.P., Neumann, A.C., Coston, J.A., Martens, C.S., Showers, W., 1992. Indicators of methane-derived carbonates and chemosynthetic organic carbon deposits: examples from the Florida Escarpment. *Palaios* 7, 361–375.
- Peckmann, J., Thiel, V., 2004. Carbon cycling at ancient methane-seeps. *Chem. Geol.* 205, 443–467.
- Peckmann, J., Gischler, E., Oschmann, W., Reitner, J., 2001. An Early Carboniferous seep community and hydrocarbon-derived carbonates from the Harz Mountains, Germany. *Geology* 29, 271–274.
- Peckmann, J., Campbell, K.A., Walliser, O.H., Reitner, J., 2007. A Late Devonian hydrocarbon-seep deposit dominated by dimerelloid brachiopods, Morocco. *Palaios* 22, 114–122.
- Peckmann, J., Birgel, D., Kiel, S., 2009. Molecular fossils reveal fluid composition and flow intensity at a Cretaceous seep. *Geology* 37, 847–850.
- Peckmann, J., Kiel, S., Sandy, M.R., Taylor, D.G., Goedert, J.L., 2011. Mass occurrences of the brachiopod *Halocrella* in late Triassic methane-seep deposits, eastern Oregon. *J. Geol.* 119, 207–220.
- Peckmann, J., Sandy, M.R., Taylor, D.G., Gier, S., Bach, W., 2013. An Early Jurassic brachiopod-dominated seep deposit enclosed by serpentinite, eastern Oregon, USA. *Palaeogeogr. Palaeoclimatol. Palaeoecol.* 390, 4–16.
- Peckmann, J., Thiel, V., Michaelis, W., Clari, P., Gaillard, C., Martire, L., Reitner, J., 1999. Cold seep deposits of Beauvoisin (Oxfordian; southeastern France) and Marmorito (Miocene; northern Italy): microbially induced authigenic carbonates. *Int. J. Earth Sci.* 88, 60–75.
- Peketi, A., Mazumdar, A., Joao, H., Patil, D., Usapkar, A., Dewangan, P., 2015. Coupled C-S-Fe geochemistry in a rapidly accumulating marine sedimentary system: diagenetic and depositional implications. *Geochem. Geophys. Geosyst.* 16, 2865–2883.
- Pickering, K., Stow, D., 1986. Inorganic major, minor, and trace element geochemistry and clay mineralogy of sediments from the Deep Sea Drilling Project Leg 96, Gulf of Mexico. *Initial Rep. Deep Sea Drill. Proj.* 96, 733–745.
- Quijada, M., Ribouleau, A., Faure, P., Michels, R., Tribouillard, N., 2016. Organic matter sulfurization on protracted diagenetic timescales: the possible role of anaerobic oxidation of methane. *Mar. Geol.* 381, 54–66.
- Roberts, H.H., Feng, D., Joye, S.B., 2010. Cold-seep carbonates of the middle and lower continental slope, northern Gulf of Mexico. *Deep-Sea Res. Part II: Top. Stud. in Oceanogr.* 57, 2040–2054.
- Rubin-Blum, M., Antony, C.P., Borowski, C., Sayavedra, L., Pape, T., Sahling, H., Bohrmann, G., Kleiner, M., Redmond, M.C., Valentine, D.L., Dublier, N., 2017. Short-chain alkanes fuel mussel and sponge *Cycloclasticus* symbionts from deep-sea gas and oil seeps. *Nat. Microbiol.* 2, 17093.
- Rumolo, P., Barra, M., Gherardi, S., Marsella, E., Sprovieri, M., 2011. Stable isotopes and C/N ratios in marine sediments as a tool for discriminating anthropogenic impact. *J. Environ. Monit.* 13, 3399–3408.
- Savard, M.M., Beauchamp, B., Veizer, J., 1996. Significance of aragonite cements around Cretaceous marine methane seeps. *J. Sediment. Res.* 66, 430–438.
- Smrzka, D., Zwicker, J., Klügel, A., Monien, P., Bach, W., Bohrmann, G., Peckmann, J., 2016. Establishing criteria to distinguish oil-seep from methane-seep carbonates. *Geology* 44, 667–670.
- Smrzka, D., Zwicker, J., Misch, D., Walkner, C., Gier, S., Monien, P., Bohrmann, G., Peckmann, J., 2019. Oil seepage and carbonate formation: a case study from the southern Gulf of Mexico. *Sedimentology* 66, 2318–2353.
- Sofer, Z., 1984. Stable carbon isotope compositions of crude oils: application to source depositional environments and petroleum alteration. *AAPG Bull.* 68, 31–49.
- Squires, R.L., Gring, M.P., 2016. Late Eocene chemosynthetic? bivalves from suspect cold seeps, Wagonwheel Mountain, central California. *J. Paleontol.* 70, 63–73.
- Suess, E., 2018. Marine cold seeps: background and recent advances. In: Wilkes, H. (Ed.), *Hydrocarbons, Oils and Lipids: Diversity, Origin, Chemistry and Fate*. Springer International Publishing, Cham, pp. 1–21.
- Tong, H., Feng, D., Peckmann, J., Roberts, H.H., Chen, L., Bian, Y., Chen, D., 2019. Environments favoring dolomite formation at cold seeps: a case study from the Gulf of Mexico. *Chem. Geol.* 518, 9–18.
- Valentine, D.L., Reddy, C.M., Farwell, C., Hill, T.M., Pizarro, O., Yoerger, D.R., Camilli, R., Nelson, R.K., Peacock, E.E., Bagby, S.C., Clarke, B.A., Roman, C.N., Soloway, M., 2010. Asphalt volcanoes as a potential source of methane to late Pleistocene coastal waters. *Nat. Geosci.* 3, 345–348.
- Wang, X.C., Chen, R.F., Whelan, J., Eglington, L., 2001. Contribution of "old" carbon from natural marine hydrocarbon seeps to sedimentary and dissolved organic carbon pools in the Gulf of Mexico. *Geophys. Res. Lett.* 28, 3313–3316.
- Werne, J.P., Lyons, T.W., Hollander, D.J., Formolo, M.J., Sinnighe Damsté, J.S., 2003. Reduced sulfur in euxinic sediments of the Cariaco Basin: sulfur isotope constraints on organic sulfur formation. *Chem. Geol.* 195, 159–179.
- Werne, J.P., Lyons, T.W., Hollander, D.J., Schouten, S., Hopmans, E.C., Sinnighe Damsté, J.S., 2008. Investigating pathways of diagenetic organic matter sulfurization using compound-specific sulfur isotope analysis. *Geochem. Cosmochim. Acta* 72, 3489–3502.
- Williscroft, K., Grasby, S.E., Beauchamp, B., Little, C.T.S., Dewing, K., Birgel, D., Poulton, T., Hryniewicz, K., 2017. Extensive Early Cretaceous (Albian) methane seepage on Ellef Ringnes Island, Canadian High Arctic. *GSA Bull.* 129, 788–805.
- Woolsey, J.R., Thomas, M.M., Robin, C.B., 2004. Gulf of Mexico Seafloor Stability and Gas Hydrate Monitoring Station Project. final technical progress report. <https://pdfs.semanticscholar.org/be9d/fbea316d2f74e8abff26a7bf728df8d3c9c.pdf>.